

A multicolor, broadband (5–20 μm), quaternary-capped InAs/GaAs quantum dot infrared photodetector

Sourav Adhikary, Yigit Aytac, Srujan Meesala, Seyoum Wolde, A. G. Unil Perera et al.

Citation: *Appl. Phys. Lett.* **101**, 261114 (2012); doi: 10.1063/1.4773373

View online: <http://dx.doi.org/10.1063/1.4773373>

View Table of Contents: <http://apl.aip.org/resource/1/APPLAB/v101/i26>

Published by the [American Institute of Physics](http://www.aip.org).

Related Articles

High efficient luminescence in type-II GaAsSb-capped InAs quantum dots upon annealing
Appl. Phys. Lett. **101**, 253112 (2012)

Polarization-resolved resonant fluorescence of a single semiconductor quantum dot
Appl. Phys. Lett. **101**, 251118 (2012)

Optical cavity efficacy and lasing of focused ion beam milled GaN/InGaN micropillars
J. Appl. Phys. **112**, 113516 (2012)

Competitive carrier interactions influencing the emission dynamics of GaAsSb-capped InAs quantum dots
Appl. Phys. Lett. **101**, 231109 (2012)

Fluorescence quantum efficiency of CdSe/ZnS quantum dots embedded in biofluids: pH dependence
J. Appl. Phys. **112**, 104704 (2012)

Additional information on *Appl. Phys. Lett.*

Journal Homepage: <http://apl.aip.org/>

Journal Information: http://apl.aip.org/about/about_the_journal

Top downloads: http://apl.aip.org/features/most_downloaded

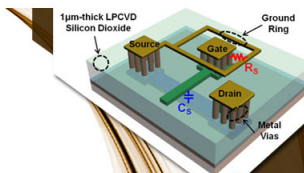
Information for Authors: <http://apl.aip.org/authors>

ADVERTISEMENT



**EXPLORE WHAT'S
NEW IN APL**

SUBMIT YOUR PAPER NOW!



SURFACES AND INTERFACES

Focusing on physical, chemical, biological, structural, optical, magnetic and electrical properties of surfaces and interfaces, and more...



ENERGY CONVERSION AND STORAGE

Focusing on all aspects of static and dynamic energy conversion, energy storage, photovoltaics, solar fuels, batteries, capacitors, thermoelectrics, and more...

A multicolor, broadband (5–20 μm), quaternary-capped InAs/GaAs quantum dot infrared photodetector

Sourav Adhikary,¹ Yigit Aytac,² Srujan Meesala,¹ Seyoum Wolde,² A. G. Unil Perera,² and Subhananda Chakrabarti^{1,a)}

¹Center for Excellence in Nanoelectronics, Department of Electrical Engineering, Indian Institute of Technology Bombay, Mumbai 400076, India

²Department of Physics & Astronomy, Georgia State University, Atlanta, Georgia 30303-4106, USA

(Received 6 August 2012; accepted 11 December 2012; published online 28 December 2012)

An InAs/GaAs quantum dot infrared photodetector with strong, multicolor, broadband (5–20 μm) photoresponse is reported. Using a combined quaternary $\text{In}_{0.21}\text{Al}_{0.21}\text{Ga}_{0.58}\text{As}$ and GaAs capping that relieves strain and maintains strong carrier confinement, we demonstrate a four color infrared response with peaks in the midwave- (5.7 μm), longwave- (9.0 and 14.5 μm), and far- (17 μm) infrared regions. Narrow spectral widths (7% to 9%) are noted at each of these wavelengths including responsivity value ~ 95.3 mA/W at 14.5 μm . Using strain field and multi-band $k \cdot p$ theory, we map specific bound-to-bound and bound-to-quasibound transitions to the longwave and midwave responses, respectively. © 2012 American Institute of Physics.

[<http://dx.doi.org/10.1063/1.4773373>]

Infrared photodetectors have numerous applications in the fields of environmental monitoring, thermal imaging, military defense and offense, and space research. Quantum dot infrared photodetectors (QDIPs) employ self-assembled InAs/GaAs quantum dots (QDs) in the active region and represent an emerging detector technology. QDIPs exploit three-dimensional confinement of carriers and atom-like discrete energy states in quantum dots to achieve low dark current levels, high operating temperature, 10–100 times longer carrier lifetimes, and normal incidence photoresponse. There are several reports on enhancement in QDIP performance by using novel heterostructure designs, most of which chiefly rely on barrier engineering. Some of these include AlGaAs^{1,2} and InGaAs^{3,4} barriers, development of an AlAs/InAs/GaAs QD superlattice structure,⁵ sub-monolayer (ML) QDs,⁶ tunneling QDIP structures,⁷ the dot-in-a-well (DWELL) recipe,⁸ dot-in-double-well heterostructure,⁹ confinement enhancing (CE) barriers,¹⁰ and quaternary InAlGaAs capping with uncoupled InGaAs QDs.¹¹ Several researchers have attempted to realize a multispectral response in a quantum well heterostructure,¹² a dot-in-well photodetector,¹³ an InGaAs/GaAs based QD intersubband transition,^{14,15} and other devices. However, QDIPs that simultaneously operate over a broad spectral range and provide superior performance are not always obtained.

In this article, we demonstrate a multicolor, broadband (5–20 μm) QDIP with narrow spectral width. The active region of our detector comprised ten layers of InAs/GaAs QDs, each with a combined quaternary (InAlGaAs) and high temperature grown GaAs capping layer. The use of a quaternary cap with a specific alloy composition, which is central to our design, enables strong carrier confinement and simultaneously helps achieve strain relief in the QD layer, thereby allowing us to realize high quality QDs. The device exhibits

a photoresponse with three prominent wavelengths (5.7, 14.5, and 17 μm) under positive bias and a four color response (5.7, 9.0, 14.5, and 17 μm) under negative bias along with narrow spectral width at each of these wavelengths. Thus, the photodetection range spans the entire midwave and longwave infrared (MWIR and LWIR) regions and the start of the far infrared (FIR) region. Using electronic structure calculations based on multi-band $k \cdot p$ theory, we identify specific intersubband transitions responsible for peaks in the experimentally observed spectral response. These simulations help validate our heterostructure design and also offer deeper insight into engineering QD intersubband transitions for strong absorption in the infrared region.

Our optimized device heterostructure (Fig. 1) consists of 10 stacked layers of InAs QDs grown on a semi-insulating (001) GaAs matrix by solid source molecular beam epitaxy (MBE). Initially, a 1.0 μm n^+ -GaAs bottom contact layer is

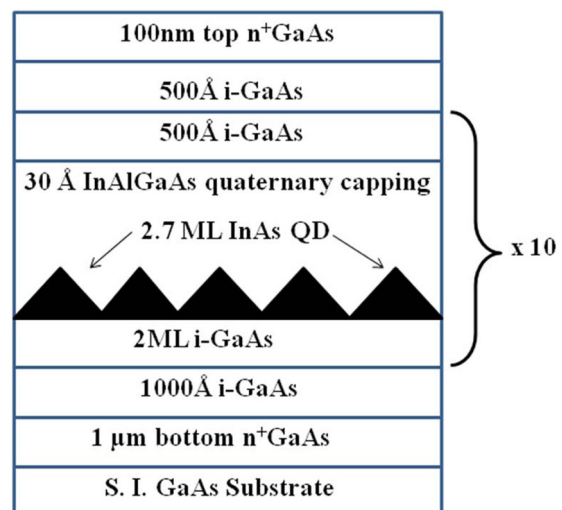


FIG. 1. Schematic of the device heterostructure depicting 10 layers of InAs/GaAs quantum dots, each capped with InAlGaAs and GaAs layers.

^{a)}Author to whom correspondence should be addressed. Electronic mail: subhanandachakrabarti@gmail.com. Tel.: +91 22 2576 7421.

grown at 590 °C. The substrate temperature is then ramped down to 520 °C for growth of 1000 Å of intrinsic GaAs. Following this, 2.7 ML InAs QDs are grown at a growth rate of 0.2 ML/s. Each dot layer is separated by a combination of a 30 Å In_{0.21}Al_{0.21}Ga_{0.58}As layer grown at 520 °C and a 500 Å GaAs layer grown at 590 °C. The composition of the quaternary alloy is chosen so that it has a band-gap that perfectly matches GaAs, according to Vegard’s law,^{16,17} thereby deliberately avoiding a dot-in-well structure.^{11,18} The sample is then capped with 500 Å of intrinsic GaAs at 520 °C, followed by a 100 nm n⁺ layer to provide a top contact. The InAlGaAs barrier in each QD layer acts as a strain induced phase-separation alloy.^{18,19} As QDs are covered by the quaternary cap, In adatoms from the alloy migrate toward the relaxed dots, resulting in a compositional In gradient across the periphery of the islands. This gradient prevents intermixing of QD and barrier material during MBE growth, thereby preserving the shape of QDs.^{18,19} After growing the quaternary cap, subsequent overgrowth of a GaAs layer at a high temperature helps smoothen the growth front for the next QD layer.

An n⁺-i-n⁺ QDIP is fabricated from the heterostructure by conventional photolithography with inductively coupled BCl₃ plasma etching for mesa pattern definition and a four-target, electron beam evaporation technique for contact metal deposition. A typical Au/Ge/Ni/Au stack is used for n⁺ Ohmic contact. Subsequently, the device is annealed at 380 °C for 1 min and bonded to a 68 pin leadless chip carrier (LCC). This carrier is mounted on the cold head of the liquid nitrogen-cooled cryostat to allow measurements of dark current, spectral response, and peak responsivity at 77 K.

Dark I-V measurements are carried out by using a Hewlett-Packard 4145 semiconductor parameter analyzer at 77 K and 100 K (Fig. 2). The dark current density value is 1.04 × 10⁻² A/cm² at 0.1 V bias. Photocurrent spectral responses are measured at 77 K by Fourier transform infrared spectroscopy (FTIR) with a glow bar source. Infrared responses spanning the entire mid- to longwave infrared range (5–20 μm) from our quaternary-capped device are shown in Figs. 3(a) and 3(b). Photoresponse peaks are

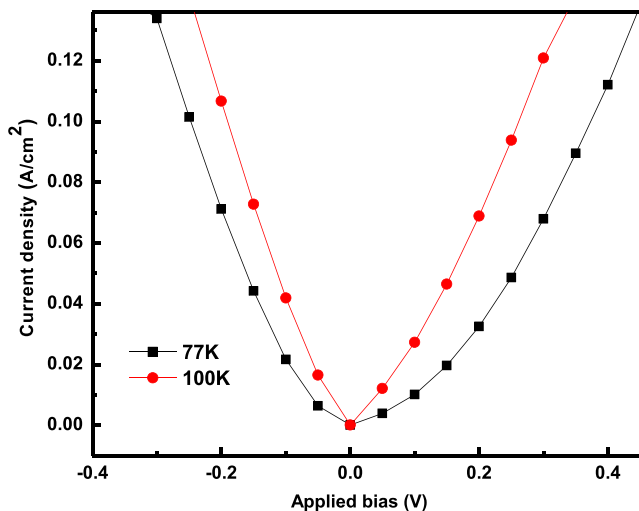


FIG. 2. Variation in dark current density of the device as a function of bias at 77 K and 100 K.

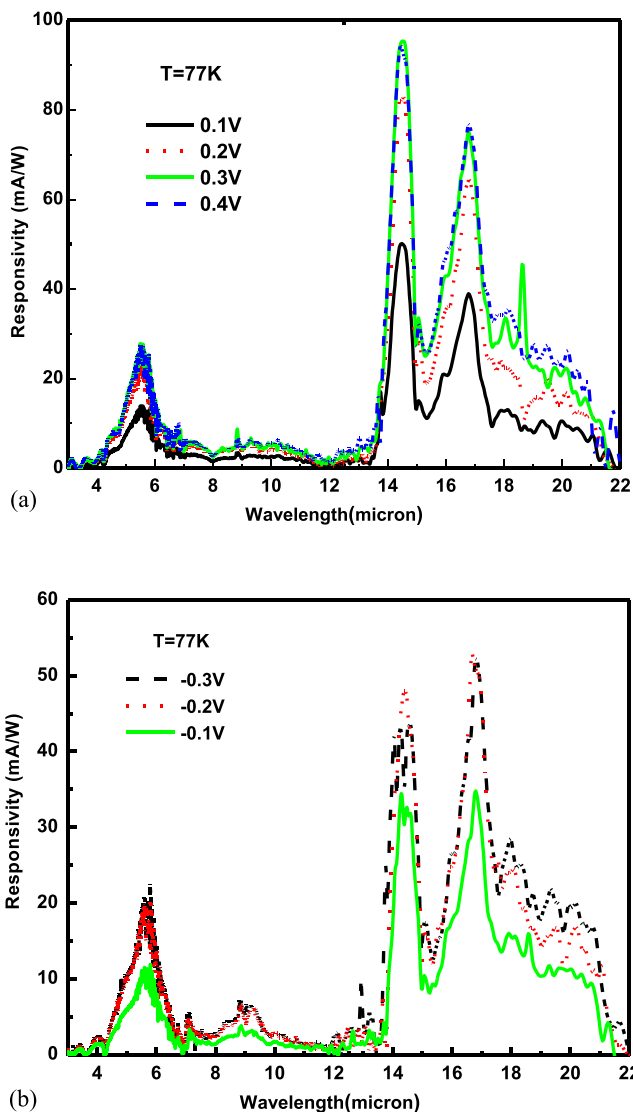


FIG. 3. (a) Three color, broadband photocurrent spectral responses of the QDIP under positive bias at 77 K, showing responsivity value ~95.3 mA/W at 14.5 μm. (b) Four color, broadband photocurrent spectral responses of the QDIP under negative bias at 77 K, showing narrow spectral width.

observed at 5.7, 9.0, 14.5, 17, and 20 μm. The peak at 9.0 μm is only dominant under negative bias. With spectral widths ($\Delta\lambda/\lambda$, where $\Delta\lambda$ is the FWHM of the peak) of ~7% and ~9%, respectively, the peaks at 14.5 and 17 μm are among the narrowest color responses.

Peak responsivity measurements are carried out using a 900 K calibrated blackbody source. The peak responsivity R_p of a QDIP is the detector output per unit of radiant input and is determined by⁹

$$R_p = \frac{I_0}{\int_{\lambda_1}^{\lambda_2} [R(\lambda)/R(\lambda_c)] L_e(\lambda, T) A_s A (t F_F / r^2) d\lambda}, \quad (1)$$

where I_0 is the photocurrent, A_s is the area of the source, L_e is the blackbody radiance, A is the area of the detector, F_F is the geometrical form factor, t is the transmission of the window, and r is the distance between the source and the detector. The responsivity corresponding to each peak wavelength is measured for both positive and negative biases, as

depicted in Figs. 3(a) and 3(b), respectively. A responsivity value of ~ 95.3 mA/W is observed (Fig. 3(a)) at 0.3 V bias, corresponding to the $14.5 \mu\text{m}$ peak. Peak responsivity values for other wavelengths are ~ 27.4 mA/W for $5.7 \mu\text{m}$ wavelength, ~ 74.6 mA/W for $17 \mu\text{m}$ wavelength under positive bias (Fig. 3(a)), and ~ 48.3 mA/W for $17 \mu\text{m}$ wavelength under negative bias (Fig. 3(b)).

To obtain further insight into the spectral characteristics of our QDIP, we compute the conduction band electronic structure of our heterostructure using strain dependent multi-band $\mathbf{k} \cdot \mathbf{p}$ theory. It has been well-established that this approach offers an accurate picture of electronic states of InAs/GaAs QDs.^{20,21} We use a truncated pyramidal geometry for the QD (Fig. 4), already used for realistic single band calculations in our earlier work.²² Strain field distribution in the quaternary capped heterostructure is computed based on the continuum mechanical model using the NEXTNANO3 software package.²³ In comparison with a plain, uncapped structure, we note that the presence of the quaternary cap leads to a slower variation of compressive strain inside the QD and a reduction in tensile strain just outside the QD boundary (Fig. 4). Fig. 4 also shows the strained conduction band profile of the heterostructure. Although the alloy composition of the capping is chosen such that its bandgap equals that of GaAs, compressive strain leads to a slight raise in the conduction band edge to about 1.6 eV. This results in stronger electron confinement, which is desirable for longer lifetime of QD bound states.

The 8-band $\mathbf{k} \cdot \mathbf{p}$ Hamiltonian for our heterostructure is written in the Kane formalism, including spin orbit splitting and the contribution from strain.²⁴ We use regular finite difference discretization in the spatial domain and harmonic averaging of material parameters²⁰ to generate a large sparse Hermitian matrix of order $8N \times 8N$, where N is the number of cells in the three-dimensional mesh. A Jacobi-Davidson algorithm based sparse matrix eigensolver²⁵ is used to diagonalize the Hamiltonian for all conduction band states below the barrier. A perusal of the envelope wave functions allows us to roughly determine the energy above which the electron states are quasi-bound (the so-called wetting layer states). The QD absorption spectrum is then calculated by summing

over the absorption due to various possible intersubband transitions

$$\alpha(E) = \frac{1}{E} \sum_{i,f} |\mathbf{e} \cdot \mathbf{M}_{if}| \exp\left(\frac{(E - E_{if})^2}{2\sigma^2}\right)$$

\mathbf{e} is the direction vector along the polarization of the incident light. $\mathbf{M}_{if} = \langle i | \mathbf{p} | f \rangle$ is the momentum matrix element of the initial and final states, and is computed approximately using the conduction band envelopes of states $|i\rangle$ and $|f\rangle$ resulting from the eigenvectors of the $\mathbf{k} \cdot \mathbf{p}$ Hamiltonian. Based on our experimental responses, we have assumed a realistic Gaussian broadening (σ) of 3% due to QD size inhomogeneity.

The calculated absorption spectrum (Fig. 5(a)), like our experimental photocurrent spectral responses, shows two distinct regions of absorption, in the midwave and longwave regions, respectively. We identify four dominant peaks in the calculated response, whose wavelengths are in good agreement with the experimental responses, thereby validating our heterostructure design. This is, to our knowledge, the first application of multi-band $\mathbf{k} \cdot \mathbf{p}$ theory that goes a step beyond fundamental electronic structure modeling of QDs by directly aiding the design of a QDIP, and subsequently, explaining the experimentally observed spectral response. Analysis of the electronic states involved in the dominant transitions in the spectrum (Fig. 5(b)) reveals that the mid-wave response ($4\text{--}11 \mu\text{m}$) is due to bound-to-quasibound transitions, while the longwave response ($14\text{--}22 \mu\text{m}$) is due to bound-to-bound transitions. Bound states (indices 2, 4, 9, 12 in Fig. 5(b)), as expected, have wave functions that are well localized inside the QD. However, it is interesting to observe that quasi-bound states (indices 25, 46 in Fig. 5(b)) are far from localized in the surrounding quaternary barrier. In fact, they have maxima at the corners of the QD. Transitions with the largest optical matrix elements are observed between states with same symmetries, for instance, 4 and 12, 2 and 46, and so on. Since bound-to-bound transitions have better wave function overlap, we expect larger optical matrix elements corresponding to them, and hence greater absorption in the longwave region. This is indeed observed in the experimental photocurrent spectra in Fig. 3.

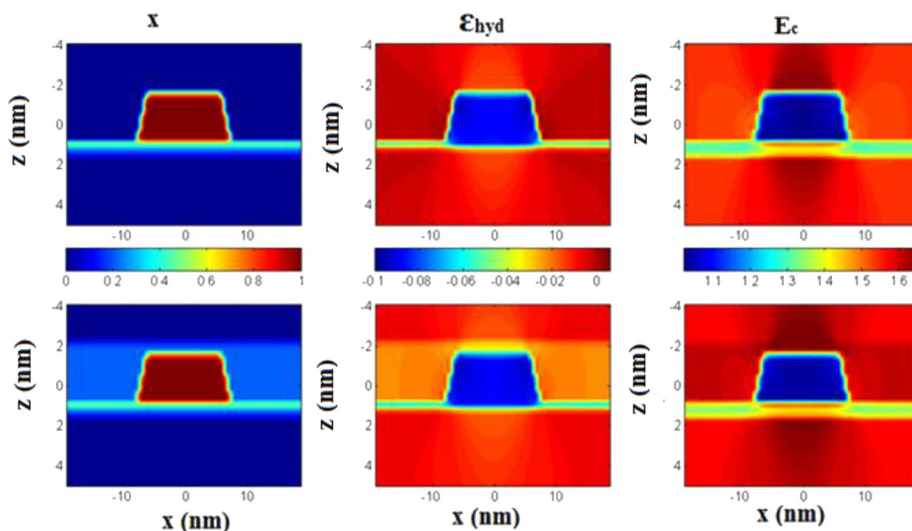


FIG. 4. From left to right, indium concentration (x), calculated hydrostatic strain (ϵ_{hyd}), and strained conduction band potential profiles (E_c) of a plain QD structure (top row) and our quaternary capped QD structure (bottom row).

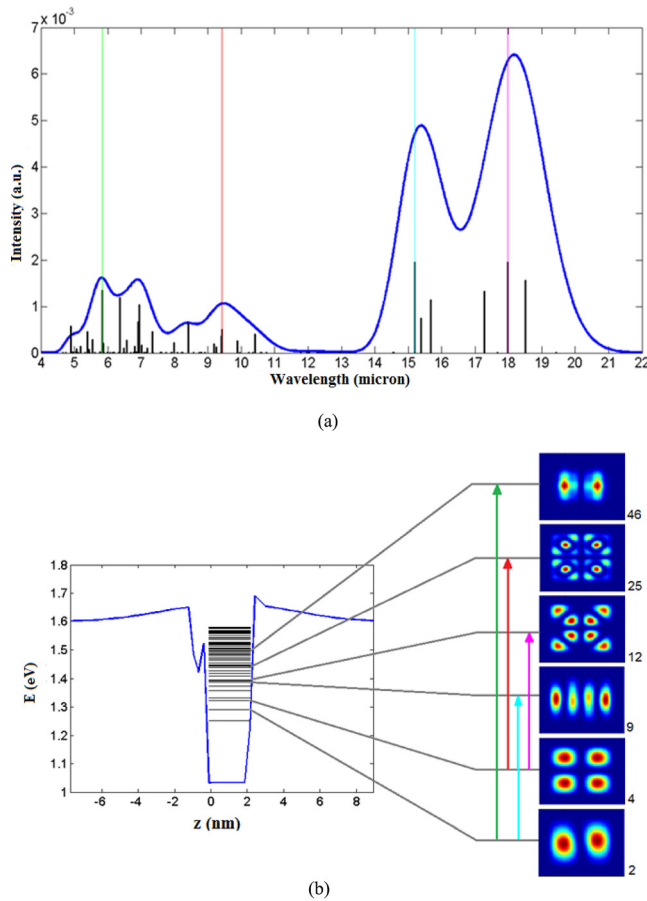


FIG. 5. (a) Theoretically computed absorption spectrum of the quaternary capped QD heterostructure. Black bars indicate wavelengths of possible intersubband transitions; their height is proportional to the magnitude of the corresponding optical matrix element. Four dominant peaks at $5.8\ \mu\text{m}$, $9.4\ \mu\text{m}$, $15.1\ \mu\text{m}$, and $18.0\ \mu\text{m}$ (indicated by colored lines) are identified in correlation with peaks in the experimental spectral response. (b) Energy spectrum of a quaternary capped QD shown along with the strained conduction band profile along the QD symmetry axis in the growth direction (001). Also shown are electronic states involved in transitions identified in (a) along with probability amplitude ($|\psi|^2$) plots of the corresponding conduction band envelopes in a horizontal cross-section of the heterostructure.

In summary, we report the design and performance of a QDIP with a combined quaternary InAlGaAs and GaAs barrier cap. Strain-driven phase separation of In from the quaternary InAlGaAs alloy prevents material inter-diffusion from QDs and preserves their shape. By using a precise quaternary alloy composition, we design a QDIP heterostructure that offers a multicolor, broadband response ($5\text{--}20\ \mu\text{m}$) cutting across mid, long, and far infrared regions, and simultaneously, narrow spectral widths. Strain field calculations of our quaternary capped QD heterostructure reveal a relatively relaxed QD layer and an elevated conduction band barrier, which leads to strong confinement of QD bound states. Heterostructure electronic states and the corresponding absorption spectrum, calculated from multi-band $k \cdot p$ theory, are in good agreement with the experimentally measured photoresponse. Further, this theoretical analysis offers fundamental insight into QDIP operation by allowing us to identify and

analyze specific types of intersubband transitions. The strong, multispectral, broadband response from our device indicates the potential of quaternary capped QDIPs for use in infrared focal plane arrays, which have a wide range of applications in environmental, military, and space imaging.

The authors acknowledge the financial support provided by the Department of Science and Technology, Government of India. Financial support was also provided by MCIT, India, through the Center of Excellence in Nanoelectronics. Additional funds from the U.S. National Science Foundation (Grant ECCS-1232184) and from the Brains and Behavior Fellowship of Georgia State University, Atlanta, Georgia, USA are also acknowledged.

- ¹A. Stiff, S. Krishna, P. Bhattacharya, and S. W. Kennerly, *IEEE J. Quantum Electron.* **37**, 1412 (2001).
- ²Z. Ye, J. C. Campbell, Z. Chen, O. Baklenov, E. T. Kim, I. Mukhametzhanov, J. Tie, and A. Madhukar, *Mater. Res. Soc. Symp. Proc.* **692**, H9.17.1 (2002).
- ³E.-T. Kim, A. Madhukar, Z. Ye, and J. C. Campbell, *Appl. Phys. Lett.* **84**, 3277 (2004).
- ⁴Z. Ye, J. C. Campbell, Z. Chen, E.-T. Kim, and A. Madhukar, *J. Appl. Phys.* **92**, 7462 (2002).
- ⁵S. Chakrabarti, A. D. Stiff-Roberts, P. Bhattacharya, and S. W. Kennerly, *Electron. Lett.* **40**, 197 (2004).
- ⁶D. Z.-Y. Ting, S. V. Bandara, S. D. Gunapala, J. M. Mumolo, S. A. Keo, C. J. Hill, J. K. Liu, E. R. Blazewski, B. Rafol, and Y.-C. Chang, *Appl. Phys. Lett.* **94**, 111107 (2009).
- ⁷X. Su, S. Chakrabarti, A. Stiff-Roberts, J. Singh, and P. Bhattacharya, *Electron. Lett.* **40**, 1082 (2004).
- ⁸S. Krishna, *J. Phys. D: Appl. Phys.* **38**, 2142 (2005).
- ⁹Y. D. Sharma, M. N. Kutty, R. V. Sheno, A. V. Barve, S. Myers, J. Shao, E. Plis, S. Lee, S. Noh, and S. Krishna, *J. Vac. Sci. Technol. B* **28**, C3G1 (2010).
- ¹⁰A. V. Barve, S. Sengupta, J. O. Kim, Y. D. Sharma, S. Adhikary, T. J. Rotter, S. J. Lee, Y. H. Kim, and S. Krishna, *Appl. Phys. Lett.* **99**, 191110 (2011).
- ¹¹S. Chakrabarti, S. Adhikary, N. Halder, Y. Aytac, and A. G. U. Perera, *Appl. Phys. Lett.* **99**, 181102 (2011).
- ¹²S. S. Li, *Int. J. High Speed Electron. Syst.* **12**, 761 (2002).
- ¹³S. Krishna, S. Raghavan, G. von Winckel, A. Stintz, G. Ariyawansa, S. G. Matsik, and A. G. U. Perera, *Appl. Phys. Lett.* **83**, 2745 (2003).
- ¹⁴S. Chakrabarti, X. H. Su, P. Bhattacharya, G. Ariyawansa, and A. G. U. Perera, *IEEE Photon. Technol. Lett.* **17**, 178 (2005).
- ¹⁵G. Ariyawansa, A. G. U. Perera, X. H. Su, S. Chakrabarti, and P. Bhattacharya, *Infrared Phys. Technol.* **50**, 156 (2007).
- ¹⁶Z. Charifi and N. Bouarissa, *Phys. Lett. A* **234**, 493 (1997).
- ¹⁷E. H. Li, *Physica E* **5**, 215 (2000).
- ¹⁸S. Adhikary, N. Halder, S. Chakrabarti, S. Majumdar, S. K. Ray, M. Herrera, M. Bonds, and N. D. Browning, *J. Cryst. Growth* **312**, 724 (2010).
- ¹⁹M. V. Maximov, A. F. Tsatsul'nikov, B. V. Volovik, D. S. Sizov, Y. M. Shernyakov, I. N. Kaiander, A. E. Zhukov, A. R. Kovsh, S. S. Mikhlin, V. M. Ustinov, Z. I. Alferov, R. Heitz, V. A. Shchukin, N. N. Ledentsov, D. Bimberg, Y. G. Musikhin, and W. Neumann, *Phys. Rev. B* **62**, 16671 (2000).
- ²⁰O. Stier, M. Grundmann, and D. Bimberg, *Phys. Rev. B* **59**, 5688 (1999).
- ²¹H. Jiang and J. Singh, *Phys. Rev. B* **56**, 4696 (1997).
- ²²M. Srujan, K. Ghosh, S. Sengupta, and S. Chakrabarti, *J. Appl. Phys.* **107**, 123107 (2010).
- ²³S. Birner, T. Zibold, T. Andlauer, T. Kubis, M. Sabathil, A. Trellakis, and P. Vogl, *IEEE Trans. Electron Devices* **54**, 2137 (2007).
- ²⁴D. Gershoni, C. H. Henry, and G. A. Baraff, *IEEE J. Quantum Electron.* **29**, 2433 (1993).
- ²⁵D. R. Fokkema, G. L. J. Sleijpen, and H. A. van der Vorst, *SIAM J. Sci. Comput.* **20**, 94 (1998).